JOURNAL OF GEOPHYSICAL RESEARCH: SOLID EARTH, VOL. 118, 4117–4126, doi:10.1002/jgrb.50213, 2013

Source properties of dynamic rupture pulses with off-fault plasticity

A.-A. Gabriel,[1,2] J.-P. Ampuero,[3] L. A. Dalguer,[1] and P. M. Mai[4]

Received 12 February 2013; revised 4 May 2013; accepted 6 May 2013; published 5 August 2013.

[1] Large dynamic stresses near earthquake rupture fronts may induce an inelastic response of the surrounding materials, leading to increased energy absorption that may affect dynamic rupture. We systematically investigate the effects of off-fault plastic energy dissipation in 2-D in-plane dynamic rupture simulations under velocity-and-state-dependent friction with severe weakening at high slip velocity. We find that plasticity does not alter the nature of the transitions between different rupture styles (decaying versus growing, pulse-like versus crack-like, and subshear versus supershear ruptures) but increases their required background stress and nucleation size. We systematically quantify the effect of amplitude and orientation of background shear stresses on the asymptotic properties of self-similar pulse-like ruptures: peak slip rate, rupture speed, healing front speed, slip gradient, and the relative contribution of plastic strain to seismic moment. Peak slip velocity and rupture speed remain bounded. From fracture mechanics arguments, we derive a nonlinear relation between their limiting values, appropriate also for crack-like and supershear ruptures. At low background stress, plasticity turns self-similar pulses into steady state pulses, for which plastic strain contributes significantly to the seismic moment. We find that the closeness to failure of the background stress state is an adequate predictor of rupture speed for relatively slow events. Our proposed relations between state of stress and earthquake source properties in the presence of off-fault plasticity may contribute to the improved interpretation of earthquake observations and to pseudodynamic source modeling for ground motion prediction.

Citation: Gabriel, A.-A., J.-P. Ampuero, L. A. Dalguer, and P. M. Mai (2013), Source properties of dynamic rupture pulses with off-fault plasticity, *J. Geophys. Res. Solid Earth*, *118*, 4117–4126, doi:10.1002/jgrb.50213.

1. Introduction

[2] Natural faults are generally surrounded by a damaged zone that might partially result from coseismic anelastic deformation [e.g., *Chester et al*., 1993]. Dynamic rupture models predict high stress concentrations at the rupture front which need to be accommodated by off-fault anelastic processes, such as plastic deformation, continuum damage, shear branching, or tensile cracks [e.g., *Kikuchi*, 1975; *Andrews*, 1976a; *Yamashita*, 2000; *Dalguer et al*., 2003a, 2003b; *Lyakhovsky et al*., 2005]. The additional energy dissipated by these processes might in turn affect key aspects of dynamic rupture and the ensuing ground motions [*Andrews*, 2005]. We consider here the role of off-fault dissipation by plastic deformation on dynamic rupture, following previous work [*Andrews*, 1976a, 2005; *Templeton and Rice*, 2008; *Duan*, 2008; *Viesca et al*., 2008; *Ma*, 2008; *Dunham et al*., 2011] but focusing on pulse-like rupture.

[3] A pre-dominance of pulse-like ruptures has been proposed based on observational earthquake source studies [e.g., *Heaton*, 1990]. However, important aspects of the dynamics of pulses are still poorly understood, for instance what controls their rise time. Here we aim at systematically quantifying the influence of plastic energy dissipation on pulse properties, such as peak slip velocity, as a function of initial stress conditions. An approximate procedure to account for off-fault plasticity in purely elastic dynamic rupture simulations was proposed by *Andrews* [2005], which involved an imposed limit to peak slip rates. Our numerical study expands the basis to calibrate such proxies.

[4] Dynamic rupture simulations are still too computationally demanding to be used routinely in the generation of broadband ground motion scenarios for earthquake engineering and seismic hazard studies. Pseudodynamic modeling is an intermediate approach between physics-based and kinematic rupture modeling. It involves kinematic source modeling with parameters constrained by dynamic source models [*Guatteri et al.*, 2004]. The importance of the correlation between source parameters (slip, rupture speed, rise time, and peak slip velocity) has been previously recog-

[1]Swiss Seismological Service, Swiss Federal Institute of Technology Zurich, Zurich, Switzerland.
[2]Now at Department of Earth and Environmental Sciences, Ludwig-Maximilians-University, Munich, Germany.
[3]Seismological Laboratory, California Institute of Technology, Pasadena, California, USA.
[4]Institute of Earth Science and Engineering, King Abdullah University of Science and Technology, Thuwal, Saudi Arabia.

Corresponding author: A.-A. Gabriel, Department of Earth and Environmental Sciences, Ludwig-Maximilians-University Munich, Theresienstrasse 41, 80333 Munich, Germany.
(gabriel@geophysik.uni-muenchen.de)

2169-9313/13/10.1002/jgrb.50213

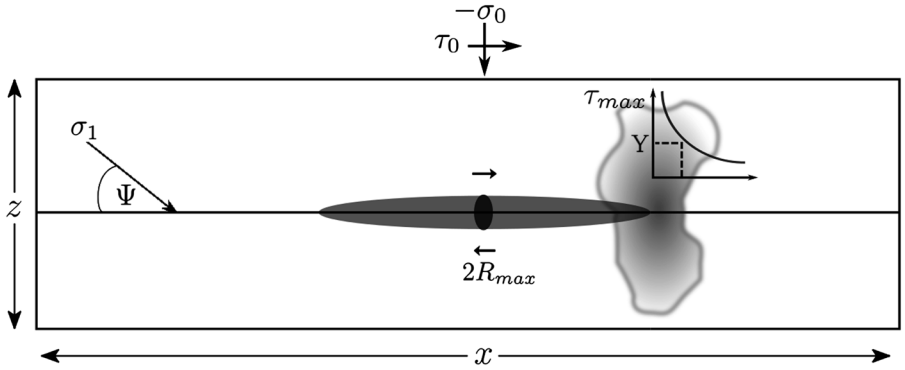

Figure 1. 2-D in-plane model setup. The fault is represented by a linear interface across which displacement discontinuity is allowed, embedded in an unbounded, isotropic, elastoviscoplastic medium. We adopt a cohesionless Coulomb yield function [*Andrews*, 2005] of internal friction μ_s (same as the static friction on the fault). Artificial nucleation is applied over a time-dependent area. Our simulations explore a wide range of maximum nucleation half-sizes $R_{\max}$, uniform initial shear stress τ_0, and angle Ψ of maximum compressive stress σ_1 axis to the fault strike.

nized and quantified [*Schmedes et al.*, 2010]. Strong ground motions in the near-source range are particularly affected by peak slip velocity and rupture speed. *Bizzarri* [2012] developed regressions between fault-averaged rupture speed and peak slip velocity, from dynamic rupture simulations in purely elastic media that lead to very large slip rates. We develop here a relation between the local values of these two quantities, accounting for the limiting effect of off-fault plasticity.

[5] Among several possible mechanisms for the generation of pulses, we consider self-healing by friction with severe velocity-weakening [e.g., *Heaton*, 1990]. This friction behavior is observed in high-speed laboratory experiments [e.g., *Tsutsumi and Shimamoto*, 1997] and predicted by thermal weakening processes such as flash heating [*Rice*, 2006]. Under such a friction law, *Gabriel et al.* [2012] found that, depending on nucleation size and background stress, dynamic ruptures in elastic media display a variety of styles. These can be classified based on their stability (decaying, steady, or growing), rupture speed (subshear or supershear), healing properties (cracks or pulses), and complexity (simple or multiple fronts).

[6] Here we study first the effect of off-fault plasticity on the selection of rupture styles, as a function of initial stress and nucleation size. We then examine self-similar growing pulses and their main kinematic properties in terms of slip gradient, peak slip velocity, rupture and healing front speed, rise time, and the contribution of off-fault plastic strain to seismic moment. We finally develop relations between the kinematic source quantities of peak slip rate and rupture velocity.

2. Model Setup

[7] We adopt the same model as in our previous work [*Gabriel et al.*, 2012] with the addition of off-fault viscoplasticity [*Andrews*, 2005; *Dunham et al.*, 2011]. We consider 2-D in-plane (plane strain) shear ruptures on a straight fault embedded in an isotropic continuum with shear modulus μ, S wave speed c_S, P wave speed c_P, and Poisson's ratio ν (Figure 1). The fault strength is governed by a rate-and-state dependent friction law with severe velocity-weakening at slip rates faster than a characteristic velocity [*Ampuero and Ben-Zion*, 2008]. The friction coefficient is determined by the slip velocity (V) and a state variable (Θ) as:

$$\mu_f = \mu_s + a\frac{V}{V+V_c} - b\frac{\Theta}{\Theta+D_c}, \tag{1}$$

where μ_s is the static friction coefficient, V_c is a characteristic velocity scale, D_c is a characteristic slip scale, and a and b are the positive coefficients quantifying a direct effect of velocity and an evolution effect, respectively. Equation (1) is equivalent to friction laws employed by *Cochard and Madariaga* [1996] and *Shaw and Rice* [2000]. The formulation is based on a simplified representation of frictional weakening caused by frictional heating [*Shaw*, 1995, 1997].

[8] The state variable has units of slip D and obeys the following evolution equation:

$$\dot{\Theta} = V - \Theta\frac{V_c}{D_c}. \tag{2}$$

Specifically, the steady state friction coefficient (obtained when $\dot{\Theta} = 0$) depends on slip velocity as

$$\mu_f(V) = \mu_d + \frac{\mu_s - \mu_d}{1+\frac{V}{V_c}}, \tag{3}$$

where a nominal dynamic friction coefficient μ_d is defined as the asymptotic value at steady state and at high slip velocity ($V \gg V_c$):

$$\mu_d = \mu_s + a - b. \tag{4}$$

[9] This form has been proposed to fit results of laboratory experiments at fast slip velocity [see, e.g., *Di Toro et al.*, 2011, and references therein] and is predicted by a flash heating model [*Rice*, 2006]. We assume a uniform initial background stress, with maximum compressive axis at an angle Ψ to the fault strike. The initial shear and normal stresses on the fault (τ_0 and σ_0, respectively) are characterized by the ratio S,

$$S = \frac{\sigma_0\mu_s - \tau_0}{\tau_0 - \sigma_0\mu_d}, \tag{5}$$

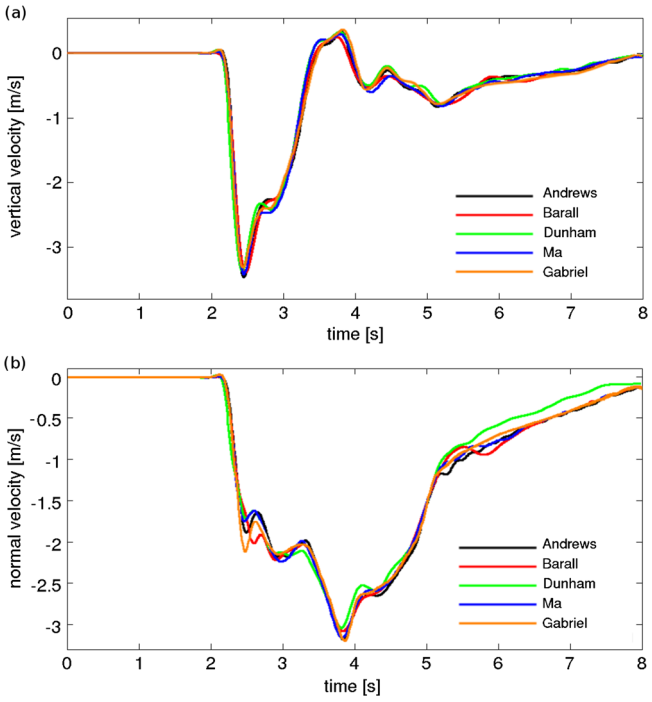

Figure 2. Results of the SCEC benchmark problem TPV13 of dynamic rupture on a dipping fault in an elastoplastic crust [*Harris et al*., 2009, 2011]. Each curve corresponds to results from a different simulation method (authors are indicated in the legend). Simulated (a) horizontal and (b) vertical ground velocity time series at a receiver 1 km away from the fault and 300 m depth, filtered with an acausal two-poles, two-passes, 3 Hz lowpass Butterworth filter.

of initial strength excess to nominal stress drop [*Das and Aki*, 1977]. We denote the nominal strength drop as

$$\tau_D = \sigma_0(\mu_s - \mu_d). \tag{6}$$

[10] We assume elastoviscoplastic behavior in the bulk, with a cohesionless Coulomb yield function of internal friction μ_s (same as the static friction on the fault). The total strain ϵ is decomposed as the sum of elastic (ϵ^e) and plastic (ϵ^p) strains:

$$\epsilon = \epsilon^e + \epsilon^p. \tag{7}$$

The adopted cohesionless Coulomb yield function for 2-D plane strain [*Andrews*, 2005] is given by

$$F(\sigma) = \tau_{\max} + \frac{1}{2}(\sigma_{xx} + \sigma_{zz})\,\sin(\phi), \tag{8}$$

where σ_{ij} denotes the components of the stress tensor, ϕ is the internal friction angle, and $\tau_{\max}$ is the maximum shear stress,

$$\tau_{\max} = \sqrt{\sigma_{xz}^2 + \frac{(\sigma_{xx} - \sigma_{zz})^2}{4}}. \tag{9}$$

To avoid grid-dependent results due to shear localization, we adopt a Perzyna-type viscous regularization. The plastic flow rule is

$$\dot{\epsilon}_{ij}^p = \frac{1}{2\mu T_v}\langle F(\sigma)\rangle \frac{\tau_{ij}}{\tau_{\max}}, \tag{10}$$

where T_v is the viscoplastic relaxation time, $< \cdot >$ denotes the Macaulay bracket (ramp function), and τ_{ij} are the components of the deviatoric stress tensor,

$$\tau_{ij} = \sigma_{ij} - \frac{1}{3}\sigma_{kk}\delta_{ij}. \tag{11}$$

The viscoplastic relaxation time (T_v), adopted to avoid mesh-dependent results, is set equal to the P wave travel time across 1.5 grid points.

[11] The focus of our work is on asymptotic properties of dynamic rupture that are independent of the nucleation process. We hence chose a computationally convenient artificial nucleation procedure building upon our previous work [*Gabriel et al.*, 2012]. We initiate ruptures by prescribing time-dependent weakening over a region that first expands and then contracts, with initial rupture speed $c_S/4$ and maximum half-size $R_{\max}$. We present our results in nondimensional form by introducing a characteristic distance,

$$L_c = \frac{\mu D_c}{\tau_D}, \tag{12}$$

and a characteristic slip rate,

$$V_{dyn} = \frac{\tau_D c_S}{\mu}. \tag{13}$$

Typically, $V_{dyn} \approx 1$ m/s and $L_c \approx 100$ m if $D_c \approx 0.1$ m.

[12] The problem is solved numerically with a spectral element method [*Ampuero*, 2008]. Figure 2 documents the agreement between our spectral element method and other methods in the Southern California Earthquake Center TPV13 benchmark problem [*Harris et al*., 2009, 2011], which involves dynamic rupture on a dipping fault with off-fault plasticity. This figure is similar to Figures 3c and 4c of [*Harris et al*., 2011], but with updated spectral element results based on a domain size large enough to avoid artificial reflections from the absorbing boundaries.

[13] We perform a large number of simulations to systematically explore the effect of initial stress level (S), stress orientation (Ψ), and nucleation half-size ($R_{\max}$) on properties of dynamic rupture with off-fault plasticity. All other model parameters are given in Table 1.

3. Results

3.1. The Effect of Off-Fault Plasticity on Rupture Styles

[14] Figure 3 summarizes the relative strength excess (S) and nucleation size ($R_{\max}$) that lead to contrasting rupture behaviors in elastic and elastoplastic media: decaying versus growing ruptures, pulse-like versus crack-like ruptures, and subshear versus supershear ruptures. Off-fault plasticity preserves the rupture styles previously found in elastic media [*Gabriel et al.*, 2012], but it systematically affects the conditions for each rupture style transition.

[15] In plastic media, the decaying-growing pulse transition requires larger $R_{\max}$ than in elastic media. Because critical nucleation sizes scale with total energy dissipation [e.g., *Day et al*., 2005, equation (34)], the additional dissipation by off-fault plasticity hinders the nucleation process, as also observed by *Dunham et al.* [2011]. We find a similar effect of plasticity on the pulse-crack transition, which *Gabriel et al.* [2012] found to operate through renucleation of slip in the hypocentral region. The limiting S value for

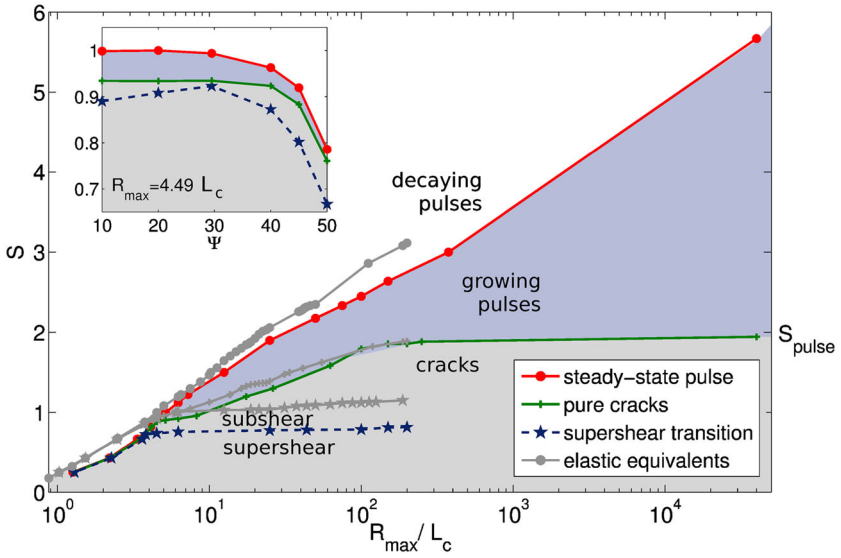

Figure 3. Rupture styles as a function of strength excess to stress drop ratio, S, and nucleation size, $R_{\max}$, in elastic (gray curves) and plastic media (colored curves) at $\Psi = 45°$. The curves indicate the conditions at the transitions between rupture styles (see legend): decaying versus growing pulses (steady state pulse), pulses versus cracks, and subshear versus supershear ruptures. The maximum S that allows cracks, according to *Zheng and Rice* [1998], is indicated as $S_{\text{pulse}} \approx 1.95$. The inset shows rupture style transitions as a function of Ψ at $R_{\max} \approx 4.5\, L_c$.

the pulse-crack transition, S_{pulse} [*Zheng and Rice*, 1998], is preserved, confirming that their theoretical arguments apply also to plastic media.

[16] In contrast, the minimal S value required for supershear ruptures is considerably reduced ($S \approx 0.8$) compared to the elastic case ($S \approx 1.2$) [see *Gabriel et al.*, 2012, section B]. Several consequences of plastic energy dissipation contribute to this result. First, as in the transitions described above, plastic dissipation hampers the nucleation of the "daughter crack" driven by dynamic stresses traveling ahead of the subshear front [*Andrews*, 1976b]. Second, off-fault plasticity limits the rupture speed (Figure 4b), which reduces the amplitude of the traveling stress peak [*Andrews*, 2005; *Dunham*, 2007]. Finally, the saturation of peak slip rate due to plasticity (Figure 4a; see also *Andrews*, 2005) shows that the velocity-dependent dynamic stress drop is also limited, which results in nominal S values lower than the actually achieved S values.

[17] The orientation of background stress determines the closeness of the prestress state to the Coulomb yield surface and hence the effectiveness of plasticity [*Templeton and Rice*, 2008; *Dunham et al.*, 2011]. All rupture style transitions have a very similar dependence on Ψ (inset of Figure 3): The transitional S values are roughly independent on Ψ when $\Psi < 30°$ and decrease with Ψ when $\Psi > 30°$.

3.2. The Effect of Off-Fault Plasticity on Pulse-Like Ruptures

[18] We now describe the interaction between self-similar growing pulses and off-fault plasticity. Figure 4 summarizes properties of growing pulse-like ruptures as a function of S with fixed $\Psi = 45°$, comparing elastic and plastic cases. The dependence of pulse properties on Ψ is shown in the insets for selected values of S.

[19] For pulses in elastic media, the peak slip rate $V_{\max}$ grows nonlinearly as a function of rupture propagation distance [*Gabriel et al.*, 2012], while in plastic media, it eventually saturates, as required by self-similarity [*Nielsen and Madariaga*, 2003]. This saturation of $V_{\max}$ induced by off-fault plasticity was first shown and explained for self-similar cracks by *Andrews* [2005]. His analysis, based on the universal asymptotic form of the stress concentration near a (subshear) rupture front, holds also for pulses. We find that the asymptotic $V_{\max}$ decreases as a function of S for $\Psi = 45°$ as shown in Figure 4a and depends on Ψ as shown in its inset for $S = 1.5$ and $S = 3$.

[20] Plasticity reduces the rupture front speed (v_r) slightly more than the healing-front speed (v_h), thus leading to overall shorter rise times (Figure 4b). In both the elastic and plastic case, v_r decreases as a function of S, while v_h is roughly constant at low S values and approaches v_r at high S values. In plastic media, this transition happens at lower S and is more pronounced: At $S > 2$, plasticity induces a transition from self-similar to steady state pulses, which propagate with constant peak slip rate, rise time, rupture speed, and off-fault plastic zone width. An increase of Ψ decreases both rupture and healing speeds uniformly (inset of Figure 4b). The dependence of the rise time gradient on S can be deduced from Figure 4b as $1/v_h - 1/v_r$: It increases distinctively with $S < 1$, as the rupture front speeds up compared to the healing front. This transition correlates with the minimal S allowing for supershear rupture, since at high healing front speeds, a certain rupture front speed is a necessary precondition for supershear rupture [*Dunham*, 2007].

[21] The total seismic moment is the sum $M_0 = M_0^s + M_0^p$ of the moment due to slip on the fault, M_0^s, and the moment due to plastic strain, M_0^p. The latter is defined as the volume integral of $\mu\sqrt{((\epsilon_{xx}^p - \epsilon_{zz}^p)/2)^2 + (\epsilon_{xz}^p)^2}$. For $\Psi = 45°$, the relative

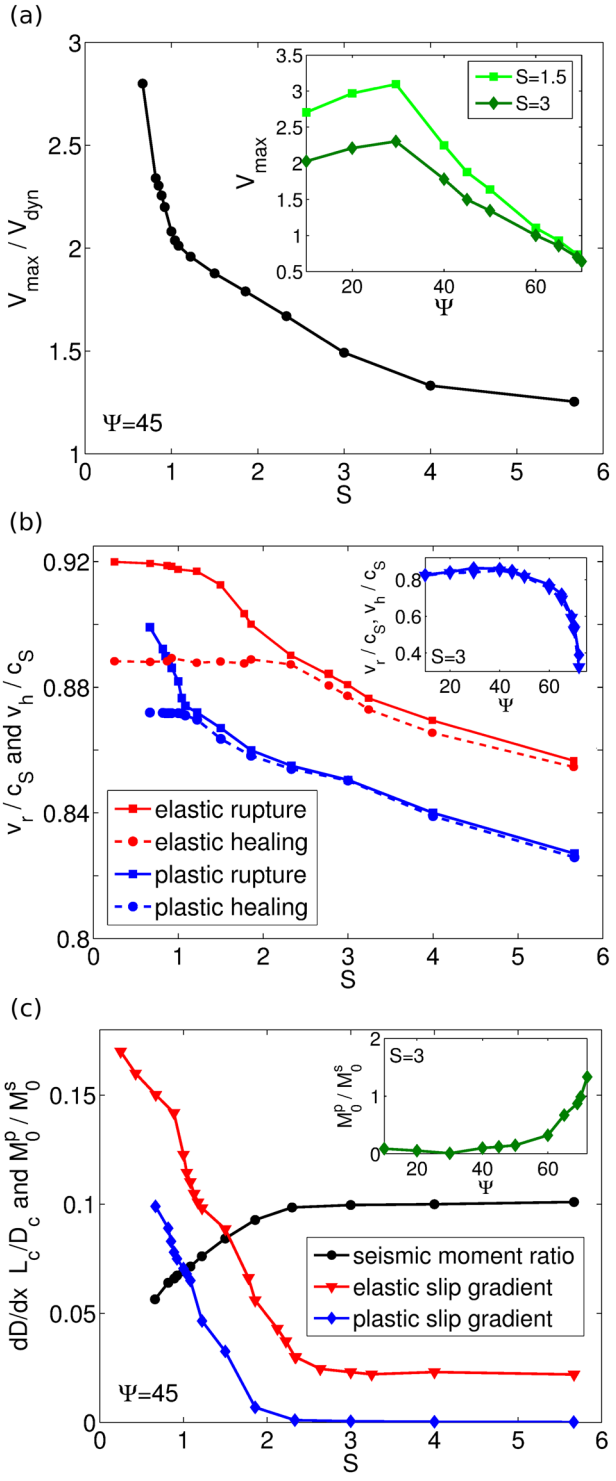

Figure 4. Properties of pulse-like ruptures, averaged over all simulations with growing pulses far away from transitions of rupture style. (a) Asymptotic peak slip rate in plastic media as a function of S for $\Psi = 45°$ and, in the inset, as a function of Ψ for $S = 1.5$ and $S = 3$. (b) Rupture and healing front speeds as a function of S for $\Psi = 45°$ and, in the inset, rise time gradient in elastic and plastic media as a function of S for $\Psi = 45°$. (c) Slip gradient in elastic and plastic media and ratio of off-fault to on-fault seismic moment in plastic media as a function of S for $\Psi = 45°$, and, in the inset, seismic moment ratio at $S = 3$ as a function of Ψ.

Table 1. Reference Simulation Parameters (Nondimensional)[a]

c_S	Shear wave speed	1
ν	Poisson's ratio	0.25
μ_s	Static friction coefficient.	0.6
μ_d	Dynamic friction coefficient.	0.1
a	Direct effect coefficient.	0.005
b	Evolution effect coefficient.	0.505
μ	Shear modulus	1
V_c	Characteristic frictional velocity scale	0.07
D_c	Characteristic frictional slip scale	1
σ_0	Background normal stress	2
τ_0	Background shear stress	0.35–1
h	Spectral element size	1
T	Nucleation duration	1–400
$R_{\max}$	**Nucleation half-size**	**0.5–4000**
S	**Relative strength**	**0.25–5.67**
Ψ	**Angle of maximum compressive stress**	**10–76**

[a]Systematically varied parameters are marked in bold.

contribution of plastic strain to the seismic moment increases as a function of S and saturates at $M_0^p/M_0^s \approx 10\%$ when $S > 2$ (Figure 4c). It also increases with increasing Ψ and becomes dominant when $\Psi > 70°$, for which the off-fault material is initially very close to failure.

[22] The dependence of rupture pulses on S is markedly different at low and high S. For $S < 1$, peak slip rate and rupture speed decrease steeply with increasing S, while for $S > 1$, they decrease more slowly. For $S < 2$, the gradient of slip decreases with S, and the ratio of off-fault to on-fault seismic moment increases, while for $S > 2$, both quantities are approximately constant.

3.3. Relation Between Peak Slip Velocity and Rupture Speed

[23] For steady state pulses, analytical relations between cohesive zone properties, background stresses, fracture energy, and rupture speed are available [*Rice et al.*, 2005] but do not account for the energy dissipated by off-fault inelastic processes. Based on our numerical findings and analytical considerations, we now develop a relation between peak slip velocity and rupture speed that potentially may be incorporated in pseudodynamic source models for ground motion calculation.

[24] In dynamic rupture models, slip velocity usually reaches its peak value in the cohesive zone, the region near the rupture front where fault weakening occurs. Within the cohesive zone, a critical slip distance, δ_c, is reached over a time equal to the cohesive zone size, ℓ_c, divided by the rupture speed, hence

$$V_{\max} \approx v_r \frac{\delta_c}{\ell_c}. \tag{14}$$

An estimate of δ_c/ℓ_c can be developed by extending classical arguments in linear elastic fracture mechanics [*Ida*, 1972, 1973] to ruptures in viscoplastic media. In elastic media, the cohesive zone is embedded in an asymptotically singular stress field characterized by a stress intensity factor K. We note that both pulses and cracks develop such a K-dominant region near their rupture front [e.g., *Freund*, 1990; *Nielsen and Madariaga*, 2003]. In elastoplastic ruptures under small scale yielding, the plastic zone is embedded in the K-dominant region. In the class of viscoplastic materials adopted here, materials with a plastic flow rule similar to

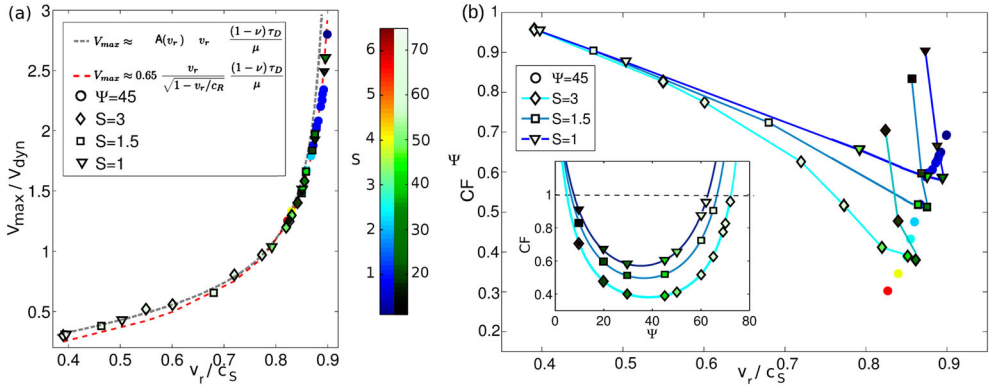

Figure 5. Relations between rupture velocity v_r, closeness to failure parameter CF [*Templeton and Rice*, 2008] and peak slip rate. (a) Peak slip rate as function of v_r under varying relative strength S and orientation of principal background stress Ψ. The dashed grey line is the relation introduced in equation (18), the dashed red line corresponds to equation (19). (b) CF versus rupture velocity v_r under varying S and Ψ. The inset shows the CF values for all our simulations. Curve colors indicate S, symbol colors indicate Ψ.

equation (10) but proportional to $\langle F(\sigma)^n \rangle$ with $1 \leq n \leq 3$, the plastic region contains a smaller zone of high strain rate characterized by another stress intensity factor, K_{tip} [*Freund and Hutchinson*, 1985; *Mataga et al.*, 1987]. This K_{tip}-dominant field controls the energy release rate at the rupture tip:

$$G_{\text{tip}} = \frac{1-\nu}{2\mu} A(v_r) K_{\text{tip}}^2, \tag{15}$$

where $A(v_r)$ is an increasing function of rupture speed given by equation (5.3.11) of *Freund* [1990]. This in turn is balanced by the fracture energy dissipated in the cohesive zone,

$$G_c = \tau_D \delta_c / 2. \tag{16}$$

The condition of finite stresses requires the stress singularity to be negated by the effect of the cohesive stresses. Assuming a steady state at the scale of the cohesive zone, i.e., neglecting the fluctuations of K_{tip}, the condition is

$$K_{\text{tip}} \approx \tau_D \sqrt{\ell_c}. \tag{17}$$

Combining equations (14) to (17) yields the following nonlinear relation between peak slip velocity and rupture speed:

$$V_{\text{max}} \approx v_r A(v_r) \frac{(1-\nu)\tau_D}{\mu}. \tag{18}$$

[25] In our self-similar pulse simulations, we find that the relation between peak slip velocity and rupture speed is well explained by equation (18) (Figure 5a). We therefore propose the following compact relation based on our data set:

$$V_{\text{max}} \approx 0.65 \frac{v_r}{\sqrt{1 - v_r/c_R}} \frac{(1-\nu)\tau_D}{\mu}, \tag{19}$$

where c_R is the Rayleigh wave speed. The prefactor 0.65 is numerically derived. Its value generally depends on the specific shape of the friction law [*Ida*, 1973]. We show in section 4.2 that the consistency between equation (19) and our simulation results does not depend on the value of the characteristic weakening velocity, V_c, which effectively tunes our friction law between slip-weakening and velocity-weakening. Figure 6 shows that the relation between peak slip rate and rupture speed developed for subshear pulses also holds for subshear cracks. For supershear ruptures, we find that a similar relation applies after replacing the Rayleigh speed by the P-wave speed and empirically adjusting the numerical prefactor to 1 (Figure 6).

3.4. Limits on Rupture Speed and Cohesive Zone Size

[26] Fracture mechanics arguments also provide a rationale for the saturation of rupture speed observed in rupture simulations with off-fault plasticity. The self-similar growth of the plastic zone induces a linear growth of the rate of plastic energy dissipation as a function of self-similar pulse width W, until plasticity eventually dominates the total energy dissipation rate G [*Andrews*, 2005]:

$$G \approx G' W, \tag{20}$$

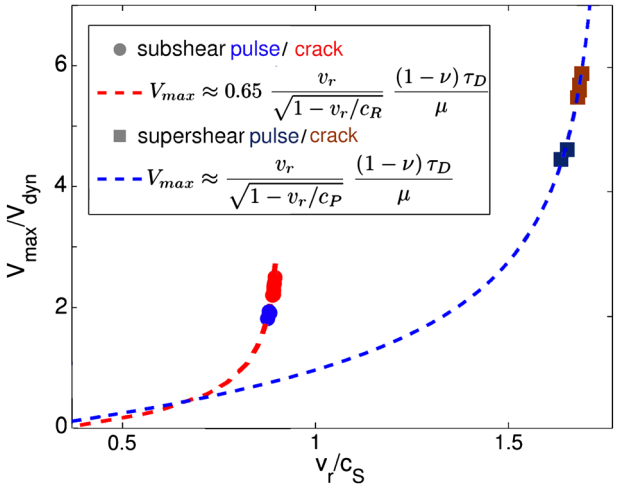

Figure 6. Asymptotic peak slip rate as a function of asymptotic rupture speed for subshear and supershear cracks and pulses (see legend) in plastic media with $\Psi = 45°$, $S = 0.92$, and varying R_{max}. The dashed curves show our proposed physics-based relations for subshear (red) and supershear (blue) ruptures. The relevant equations are given in the legend and are modified versions of equation (19) in the main text.

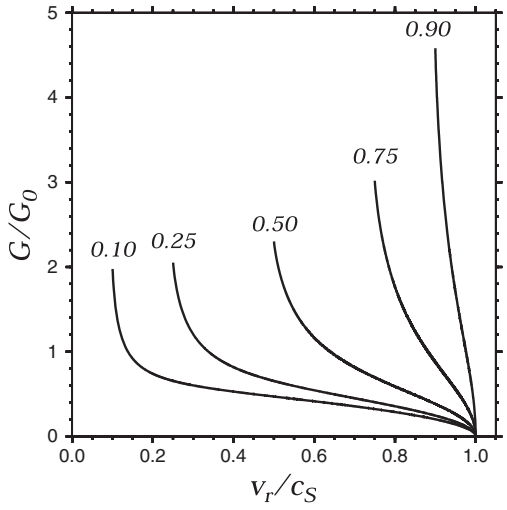

Figure 7. Energy release rate at the rupture front of a self-similar pulse in mode III, normalized by $G_0 = \pi\Delta\tau^2 W/2\mu$, as a function of rupture speed v_r (normalized by S wave speed c_S) for five different values of the ratio between healing and rupture speeds, v_h/v_r (see labels on each curve). From *Ruiz* [2007], based on results by *Nielsen and Madariaga* [2003].

where the constant gradient $G' = dG/dW$ depends on Ψ and S. The energy release rate of self-similar pulse-like ruptures can be expressed as:

$$G = C\, k_w(v_r, v_h)\Delta\tau^2 W\frac{1-\nu}{2\mu}, \tag{21}$$

where C is a constant of order 1, $k_w(v_r, v_h)$ is a function of rupture speed and of the speed of the healing front, and $\Delta\tau$ refers to the dynamic stress drop [*Nielsen and Madariaga*, 2003]. Combining equations (20) and (21) leads to:

$$k_w(v_r, v_h) = \frac{2\mu G'}{C(1-\nu)\Delta\tau^2}. \tag{22}$$

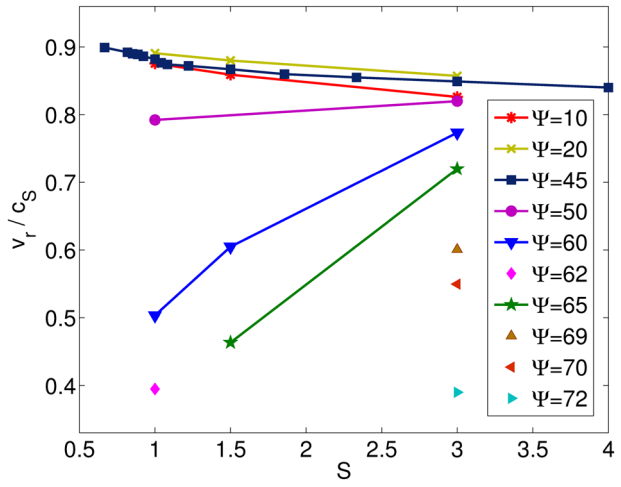

Figure 8. Rupture speed v_r/c_S as a function of S for Ψ = 10° to 72° from the simulations shown in Figure 5b. Curve colors indicate Ψ (see legend).

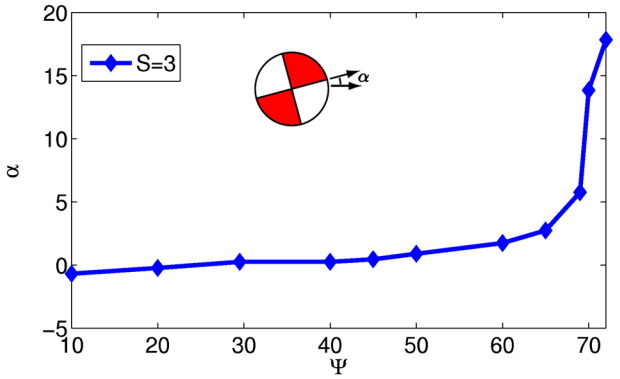

Figure 9. Rotation angle (α) of the total seismic moment (the combined effect of fault slip and off-fault plastic strain) with respect to the fault plane, as a function of the prestress angle (Ψ) for $S = 3$.

The function k_w can be derived from results by *Dunham* [2007], section B1, and *Broberg* [1999], p. 418. It is a bounded and monotonically decreasing function of v_r, with $k_w = 0$ if $v_r = c_R$. For reference, Figure 7 shows k_w in mode III. Hence, if the right-hand side of equation (22) is small enough, then a unique solution for v_r for any given v_h is obtained, and this limiting speed is smaller than the Rayleigh speed. This implies that steady rupture speed slower than the usual subshear limiting speed c_R may result from self-similar energy dissipation.

[27] The argument can similarly be developed for steady pulses and self-similar cracks. The function k_w then depends only on rupture speed [*Freund*, 1990; *Rice et al.*, 2005]. For crack-like rupture, rupture propagation distance must be considered instead of the pulse width W.

[28] To ultimately enable the prediction of rupture speed, a relation is needed between the gradient of energy dissipation rate G' and model parameters such as S or Ψ. Available results for dynamic fracture in viscoplastic media are unfortunately limited to materials with pressure-independent yield [*Freund and Hutchinson*, 1985; *Mataga et al.*, 1987]. *Templeton and Rice* [2008] introduced a closeness to failure (CF) parameter that measures the proximity of the initial state of stress to the plastic yield surface. For cohesionless materials, it can be expressed as

$$\mathrm{CF} = \frac{(\mu_s + S\mu_d)/\sin(\phi)}{(1+S)\sin(2\Psi) + (\mu_s + S\mu_d)\cos(2\Psi)}. \tag{23}$$

We find that CF is a good predictor of the combined effect of Ψ and S on rupture speed for ruptures slower than $\approx 0.6\, c_S$ and $\Psi > 30°$ (Figure 5b). Faster ruptures have a more complicated dependence on Ψ and S. High values of CF do not lead to slow ruptures at low $\Psi < 30°$, due to a reduced efficiency of transient stresses to sustain plastic yield [*Dunham et al.*, 2011]. Rupture speed decreases with S if $\Psi \leq 45°$ but increases with S if $\Psi \geq 50°$ (see Figure 8).

[29] Combining equations (15) to (17) leads to

$$\ell_c \approx \frac{\mu\delta_c}{A(v_r)(1-\nu)\tau_D}. \tag{24}$$

Considering the saturation of rupture speed, this equation shows that the size of the process zone also saturates, as reported in numerical simulations by *Hok et al.* [2010]. It is

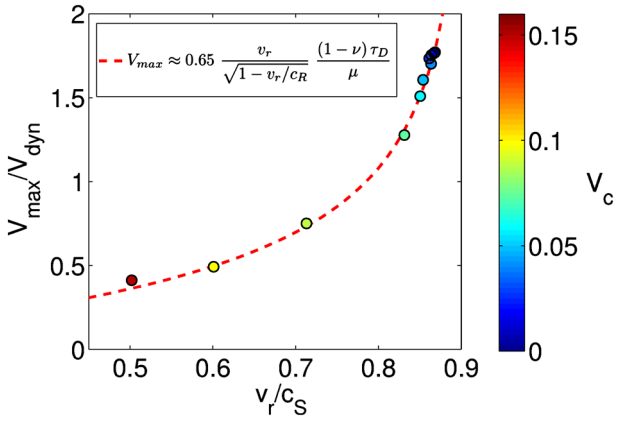

Figure 10. Asymptotic peak slip rate as function of rupture speed for subshear cracks and pulses at $\Psi = 45°$, $S = 3$, $R_{\max} = 400\,L_c$, and characteristic weakening velocity V_c ranging from 0.01 to 0.15 V_{dyn} (see color scale). The dashed line represents our equation (19).

significant that the Lorentz contraction of the process zone is prevented in self-similar ruptures in viscoplastic media despite the growth of the outer-scale stress intensity factor K with rupture distance.

4. Discussion

4.1. Interpreting Earthquake Source Observations

[30] Our quantitative relations between the state of stress and source properties provide an innovative framework for interpreting earthquake observations. For instance, at moderate to large angles Ψ between the maximum compressive stress and the fault strike, ruptures are significantly slower when the initial stress state is closer to failure (smaller S). In contrast, at lower Ψ, faster ruptures are associated with larger initial stresses (see Figure 8). A correlation between high stress drop and low rupture speed has been inferred from seismological observations of the 2003 Big Bear sequence [*Tan and Helmberger*, 2010], implying a large angle Ψ in this region.

[31] Accounting for off-fault plasticity in earthquake rupture simulations imposes physical limits on extreme ground motion: plastic dissipation limits the rupture speed and peak slip rate of pulses. We quantify how the amplitude and orientation of initial stresses affect these limiting values. Furthermore, equation (19) correlates peak slip rate directly with strength drop, and thus effective normal stress, which implies a depth dependence of the limiting peak slip rate (as proposed by *Andrews* [2005]). The development of reliable observations of peak slip rate and rupture speed could provide a constraint on dynamic strength drop, an otherwise elusive parameter.

[32] We also find that at low background stresses, plasticity induces a steady state behavior of pulse-like rupture. Then, if the background stress is close to failure, the contribution of plastic strain to the total seismic moment is significant and may appreciably distort the earthquake moment tensor. Figure 9 shows that the rotation angle of the total moment tensor reaches up to 18° for the ruptures with high Ψ. Thus, the seismic moment of relatively slow earthquakes (40% to 60% of c_S) might be dominated by the off-fault plastic strain contribution in faults oriented at large Ψ, as, e.g., $\Psi = 77°$ on the Calaveras fault [*Schaff et al.*, 2002].

4.2. Validity of the Relation Between Peak Slip Rate and Rupture Speed for Other Friction Behaviors

[33] The friction law adopted in this work is a minimalistic mathematical formulation that yet encapsulates a fundamental ingredient of natural faulting: severe velocity-weakening at high slip rate. Our qualitative results on interactions between slip pulses and off-fault dissipation should also apply to other fault constitutive equations, as long as they generate self-healing pulse-like ruptures with a small "breakdown zone." In the simulations presented, so far, we assumed that the characteristic velocity of the friction law is $V_c = 0.07\,V_{dyn}$. As discussed by [*Gabriel et al.*, 2012], this parameter may span a broad range of values in natural faults and tunes the weakening mechanism between two

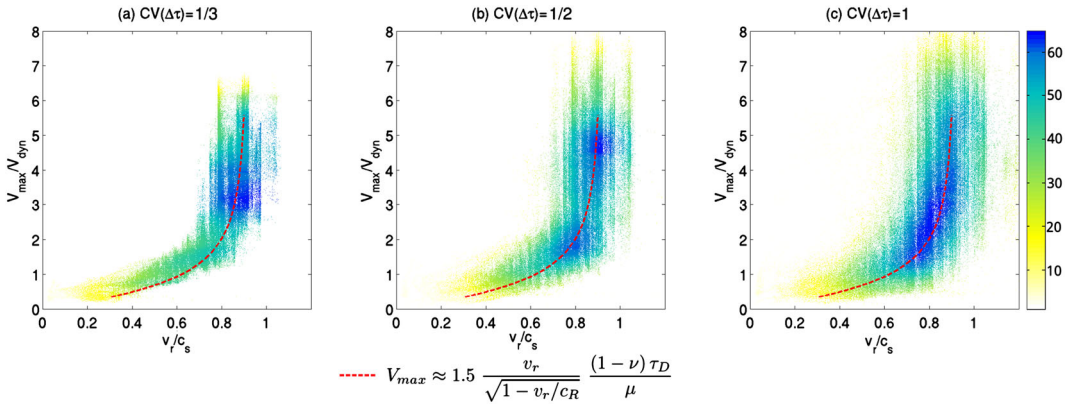

Figure 11. Relation between peak slip rate and rupture speed in three 3-D rupture simulations by *Song and Dalguer* [2013], which assumed slip-weakening friction and heterogeneous initial stresses. For each simulation, the coefficient of variation of the nominal stress drop, $CV(\Delta\tau)$, defined as the ratio of its standard deviation to its mean (3 MPa), is indicated above the respective figure. The color scale indicates the absolute density of data points. The dashed red line is a relation similar to our equation (19), but with a different prefactor.

extreme behaviors: slip-weakening and velocity-weakening. We test the generality of our observations for a set of simulations, by varying V_c/V_{dyn} from 0.01 to 0.15 (Figure 10). The simulation with $V_c/V_{dyn} = 0.06$ results in pulse-like rupture, whereas lower values of V_c result in crack-like ruptures. We find that the peak slip rates and rupture velocities are still related by equation (19) (see the dashed red line in Figure 10).

4.3. Validity of the Relation Between Peak Slip Rate and Rupture Speed Under Heterogeneous Stress in 3-D

[34] Our model is deliberately simplified in order to expose the potential effects of off-fault plasticity on earthquake dynamics. Nevertheless, the influence of plasticity in the presence of other sources of complexity, such as 3-D effects, heterogeneities, and thermal or fluid coupling, is an important question. We address specifically 3-D and heterogeneous initial stress effects in Figure 11, based on a set of dynamic rupture simulations by *Song and Dalguer* [2013]. These authors considered spatial distributions of stress drop with $1/k$ spectral decay and Gaussian probability density function with mean stress drop of 3 MPa and standard deviation ranging from 1 MPa to 3 MPa. They assumed constant slip-weakening distance (0.25 m), constant strength excess (4.5 MPa, $S = 1.5$), a homogeneous elastic half-space, and artificial nucleation by setting a negative strength excess (5% of the stress drop) on a circular patch (which is excluded from Figure 11). Other relevant modeling parameters are summarized in their Table 1. Figure 11 indicates that equation (19), after adjusting the numerical prefactor to 1.5, is consistent with the relation between peak slip rate and rupture speed found in these 3-D dynamic rupture models under linear slip-weakening friction and highly heterogeneous initial stress. The scatter around this relation is partly due to the fact that mode I, mode II, and mixed-mode rupture fronts follow similar relations separately, but with different prefactors and limiting speeds.

5. Conclusions

[35] We conducted numerical simulations to quantify the effect of off-fault plasticity on the style of dynamic ruptures and on asymptotic properties of self-similar pulses under strong velocity-weakening friction. Off-fault plasticity preserves the rupture styles, and underlying transition mechanisms found in elastic media [*Gabriel et al.*, 2012]. Plastic energy dissipation increases the minimum stress (decreases S, the ratio of initial strength excess to nominal stress drop) and increases the nucleation size ($R_{\max}$) required for self-sustained ruptures and for supershear ruptures. In contrast, off-fault plasticity increases the nucleation size but does not affect the minimum stress required for crack-like ruptures.

[36] We found that the numerically observed nonlinear relation between peak slip velocity and rupture speed can be understood by dynamic fracture mechanics concepts. This result is consistent with the strong correlation between rupture velocity and peak slip rate observed in dynamic rupture models by *Schmedes et al.* [2010] and *Bizzarri* [2012]. The derived relation is valid for subshear cracks and, slightly modified, for supershear ruptures but is not expected to hold for coalescing rupture fronts.

[37] Our study captures fundamental processes governing pulse-like rupture propagation coupled to self-similar off-fault energy dissipation. The relations found here between the background state of stress and the limits on rupture speed and peak slip velocity imposed by off-fault plasticity may encapsulate a major effect of plastic deformation on near-field ground motions. Thus, our results may be a suitable starting point to develop new pseudodynamic source parametrizations for source inversion and ground motion prediction that account for off-fault plasticity.

[38] **Acknowledgments.** This work was supported by PG&E, NSF (grant EAR-0944288), and SCEC (funded by NSF EAR-0106924 and USGS 02HQAG0008 cooperative agreements). This is SCEC contribution number 1655. We acknowledge the research computing facilities at King Abdullah University of Science and Technology and J. Ruiz for providing Figure 7. We thank the Editor and the editorial team, E.M. Dunham, and an anonymous reviewer for their improvements of the manuscript.

References

Ampuero, J. P. (2008), SEM2DPACK*, A Spectral Element Method Tool for 2D Wave Propagation and Earthquake Source Dynamics,* User's guide, version 2.3.0.

Ampuero, J. P., and Y. Ben-Zion (2008), Cracks, pulses, and macroscopic asymmetry of dynamic rupture on a bimaterial interface with velocity-weakening friction, *Geophys. J. Int.*, *173*(2), 674–692, doi:10.1111/j.1365-246X.2008.03736.x.

Andrews, D. J. (1976a), Rupture velocity of plane strain shear cracks, *J. Geophys. Res.*, *81*, 5679–5689, doi:10.1029/JB081i032p05679.

Andrews, D. J. (1976b), Rupture propagation with finite stress in antiplane strain, *J. Geophys. Res.*, *81*(20), 3575–3582, doi:10.1029/JB081i020p03575.

Andrews, D. J. (2005), Rupture dynamics with energy loss outside the slip zone, *J. Geophys. Res.*, *110*, B01307, doi:10.1029/2004JB003191.

Bizzarri, A. (2012), Rupture speed and slip velocity: What can we learn from simulated earthquakes?, *Earth Planet. Sci. Lett.*, *317–318*, 196–203, doi:10.1016/j.epsl.2011.11.023.

Broberg, K. B. (1999), *Cracks and Fracture*, Academic Press, London, U.K.

Chester, F. M., J. P. Evans, and R. L. Biegel (1993), Internal structure and weakening mechanisms of the San Andreas Fault, *J. Geophys. Res.*, *98*, 771–786, doi:10.1029/92JB01866.

Cochard, A., and R. Madariaga (1996), Complexity of seismicity due to highly rate-dependent friction, *J. Geophys. Res.*, *101*(B11), 321–325, doi:10.1029/96JB02095.

Dalguer, L. A., K. Irikura, and J. D. Riera (2003a), Generation of new cracks accompanied by the dynamic shear rupture propagation of the 2000 Tottori (Japan) earthquake, *Bull. Seismol. Soc. Am.*, *93*, 2236–2252, doi:10.1785/0120020171.

Dalguer, L. A., K. Irikura, and J. D. Riera (2003b), Simulation of tensile crack generation by three-dimensional dynamic shear rupture propagation during an earthquake, *J. Geophys. Res.*, *108*(B3), 2144, doi:10.1029/2001JB001738.

Das, S., and K. Aki (1977), Fault plane with barriers: A versatile earthquake model, *J. Geophys. Res.*, *82*(36), 5658–5670, doi:10.1029/JB082i036p05658.

Day, S. M., L. A. Dalguer, N. Lapusta, and Y. Liu (2005), Comparison of finite difference and boundary integral solutions to three-dimensional spontaneous rupture, *J. Geophys. Res.*, *110*(B12), 307, doi:10.1029/2005JB003813.

Di Toro, G., R. Han, T. Hirose, N. De Paola, S. Nielsen, K. Mizoguchi, F. Ferri, M. Cocco, and T. Shimamoto (2011), Fault lubrication during earthquakes, *Nature*, *471*, 494–498, doi:10.1038/nature09838.

Duan, B. (2008), Effects of low-velocity fault zones on dynamic ruptures with nonelastic off-fault response, *Geophys. Res. Lett.*, *35*, L04307, doi:10.1029/2008GL033171.

Dunham, E. (2007), Conditions governing the occurrence of supershear ruptures under slip-weakening friction, *J. Geophys. Res.*, *112*(B7), 1–24, doi:10.1029/2006JB004717.

Dunham, E. M., D. Belanger, L. Cong, and J. E. Kozdon (2011), Earthquake ruptures with strongly rate-weakening friction and off-fault plasticity, Part 1: Planar faults, *Bull. Seismol. Soc. Am.*, *101*(5), 2296–2307, doi:10.1785/0120100075.

Freund, L. (1990), *Dynamic Fracture Mechanics*, Cambridge Monographs on Mechanics and Applied Mathematics, Cambridge University Press, Cambridge, U.K.

Freund, L., and J. Hutchinson (1985), High strain-rate crack growth in rate-dependent plastic solids, *J. Mech. Phys. Solids*, *33*(2), 169–191, doi:10.1016/0022-5096(85)90029-8.

Gabriel, A.-A., J.-P. Ampuero, L. A. Dalguer, and P. M. Mai (2012), The transition of dynamic rupture modes in elastic media under velocity-weakening friction, *J. Geophys. Res.*, *117*(B9), 0148–0227, doi:10.1029/2012JB009468.

Guatteri, M., P. M. Mai, and G. C. Beroza (2004), A pseudo-dynamic approximation to dynamic rupture models for strong ground motion prediction, *Bull. Seismol. Soc. Am.*, *94*(6), 2051–2063, doi:10.1785/0120040037.

Harris, R. A., et al. (2009), The SCEC/USGS dynamic earthquake rupture code verification exercise, *Seismol. Res. Lett.*, *80*(1), 119–126, doi:10.1785/gssrl.80.1.119.

Harris, R. A., et al. (2011), Verifying a computational method for predicting extreme ground motion, *Seismol. Res. Lett.*, *82*(5), 638–644, doi:10.1785/gssrl.82.5.638.

Heaton, T. H. (1990), Evidence for and implications of self-healing pulses of slip in earthquake rupture, *Phys. Earth Planet. Inter.*, *64*(1), 1–20, doi:10.1016/0031-9201(90)90002-F.

Hok, S., M. Campillo, F. Cotton, P. Favreau, and I. Ionescu (2010), Off-fault plasticity favors the arrest of dynamic ruptures on strength heterogeneity: Two-dimensional cases, *Geophys. Res. Lett.*, *37*(2), 1944–8007, doi:10.1029/2009GL041888.

Ida, Y. (1972), Cohesive force across the tip of a longitudinal-shear crack and Griffith's specific surface energy, *J. Geophys. Res.*, *77*(20), 3796–3805, doi:10.1029/JB077i020p03796.

Ida, Y. (1973), The maximum acceleration of seismic ground motion, *Bull. Seismol. Soc. Am.*, *63*(3), 959–968.

Kikuchi, M. (1975), Inelastic effects on crack propagation, *J. Phys. Earth*, *23*, 161–172.

Lyakhovsky, V., Y. Ben-Zion, and A. Agnon (2005), A viscoelastic damage rheology and rate- and state-dependent friction, *Geophys. J. Int.*, *161*(1), 179–190, doi:10.1111/j.1365-246X.2005.02583.x.

Ma, S. (2008), A physical model for widespread near-surface and fault zone damage induced by earthquakes, *Geochem. Geophys. Geosyst.*, *9*, Q11009, doi:10.1029/2008GC002231.

Mataga, P., L. Freund, and J. Hutchinson (1987), Crack tip plasticity in dynamic fracture, *J. Phys. Chem. Solids*, *48*, 985–1005, doi:10.1016/0022-3697(87)90115-6.

Nielsen, S., and R. Madariaga (2003), On the self-healing fracture mode, *Bull. Seismol. Soc. Am.*, *93*(6), 2375–2388.

Rice, J. R. (2006), Heating and weakening of faults during earthquake slip, *J. Geophys. Res.*, *111*(10), B05311, doi:10.1029/2005JB004006.

Ruiz, J. (2007), Modeling broadband strong ground motion by kinematic modeling of extended sources: Application to Santiago City, Chile, PhD Thesis, IPG Paris.

Rice, J. R., C. G. Sammis, and R. Parsons (2005), Off-fault secondary failure induced by a dynamic slip pulse, *Bull. Seismol. Soc. Am.*, *95*(1), 109–134, doi:10.1785/0120030166.

Schaff, D. P., G. H. R. Bokelmann, G. C. Beroza, F. Waldhauser, and W. L. Ellsworth (2002), High-resolution image of Calaveras Fault seismicity, *J. Geophys. Res.*, *107*(B9), 2186, doi:10.1029/2001JB000633.

Schmedes, J., R. J. Archuleta, and D. Lavallée (2010), Correlation of earthquake source parameters inferred from dynamic rupture simulations, *J. Geophys. Res.*, *115*, B03304, doi:10.1029/2009JB006689.

Shaw, B. E. (1995), Frictional weakening and slip complexity on earthquake faults, *J. Geophys. Res.*, *100*(B9), 18,239–18,251.

Shaw, B. E. (1997), Model quakes in the two dimensional wave equation, *J. Geophys. Res.*, *102*(B12), 27,367–27,377, doi:10.1029/97JB02786.

Shaw, B. E., and J. R. Rice (2000), Existence of continuum complexity in the elastodynamics of repeated fault ruptures, *J. Geophys. Res.*, *105*(B10), 23,791–23,810, doi:10.1029/2000JB900203.

Song, S., and L. A. Dalguer (2013), Importance of 1-point statistics in earthquake source modeling for ground motion simulation, *Geophys. J. Int.*, *192*, 1255–1270, doi:10.1093/gji/ggs089.

Tan, Y., and D. Helmberger (2010), Rupture directivity characteristics of the 2003 Big Bear sequence, *Bull. Seismol. Soc. Am.*, *100*(3), 1089–1106, doi:10.1785/0120090074.

Templeton, E. L., and J. R. Rice (2008), Off-fault plasticity and earthquake rupture dynamics: 1. Dry materials or neglect of fluid pressure changes, *J. Geophys. Res.*, *113*, B09306, doi:10.1029/2007JB005529.

Tsutsumi, A., and T. Shimamoto (1997), High-velocity frictional properties of gabbro, *Geophys. Res. Lett.*, *24*(6), 699–702.

Viesca, R. C., E. L. Templeton, and J. R. Rice (2008), Off-fault plasticity and earthquake rupture dynamics: 2. Effects of fluid saturation, *J. Geophys. Res.*, *113*, B09307, doi:10.1029/2007JB005530.

Yamashita, T. (2000), Generation of microcracks by dynamic shear rupture and its effects on rupture growth and elastic wave radiation, *Geophys. J. Int.*, *143*(2), 395–406, doi:10.1046/j.1365-246X.2000.01238.x.

Zheng, G., and J. Rice (1998), Conditions under which velocity-weakening friction allows a self-healing versus a cracklike mode of rupture, *Bull. Seismol. Soc. Am.*, *88*(6), 1466–1483.